

Limits of BOSS DFT: O2 + Al(111) dynamics on a screened hybrid Van der Waals DFT potential energy surface

Bree, R.A.B. van; Kroes, G.J.

Citation

Bree, R. A. B. van, & Kroes, G. J. (2025). Limits of BOSS DFT: O2 + Al(111) dynamics on a screened hybrid Van der Waals DFT potential energy surface. *The Journal Of Physical Chemistry C*, 129(11), 5408-5421. doi:10.1021/acs.jpcc.5c00327

Version: Publisher's Version

License: <u>Creative Commons CC BY 4.0 license</u>
Downloaded from: <u>https://hdl.handle.net/1887/4281745</u>

Note: To cite this publication please use the final published version (if applicable).

pubs.acs.org/JPCC

Article

Limits of BOSS DFT: O₂ + Al(111) Dynamics on a Screened Hybrid Van der Waals DFT Potential Energy Surface

R. A. B. van Bree* and G. J. Kroes*



Downloaded via LEIDEN UNIV on November 3, 2025 at 13:04:34 (UTC). See https://pubs.acs.org/sharingguidelines for options on how to legitimately share published articles.

Cite This: J. Phys. Chem. C 2025, 129, 5408-5421



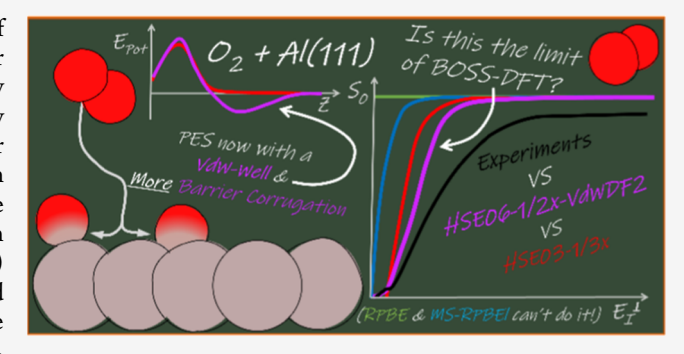
ACCESS I

Metrics & More

Article Recommendations

Supporting Information

ABSTRACT: The activated dissociative chemisorption (DC) of O₂ on Al(111) is a thoroughly studied benchmark system for oxygen-metal interactions. However, research based on density functional theory (DFT) has not yet been able to accurately determine the electronic structure, and theory as a whole has so far been unable to reproduce measured sticking probabilities with chemical accuracy. Previous work has argued that this is likely due to the inability of DFT at the generalized gradient approximation (GGA) level to describe the barriers to DC of O2 on Al(111) correctly. The argument is that the most commonly applied electronic structure approach in surface science, which involves the use of GGA-DFT, yields too low reaction barriers for the DC of O₂



on Al(111). Moreover, it seems that GGAs will generally fail to accurately predict barriers for systems with low charge transfer energy, i.e., systems for which charge transfer from metal to molecule at the transition state is likely. Subsequent work on both O₂ + Al(111) and $O_2 + Cu(111)$ has suggested that screened hybrid density functionals (DF) yield more accurate barrier heights for DC on metal surfaces. However, so far the use of only a screened hybrid DF was not enough to ensure a highly accurate description for O_2 + Al(111). Even though the onset of the sticking probability (S_0) curve was correctly described, the slope, or width, of the curve was not. The use of a nonlocal correlation DF combined with an increased fraction of exact exchange in the screened hybrid exchange DF was believed to further improve the description of the electronic structure by increasing the energetic corrugation of the barrier. This approach was assumed to increase the width of the sticking curve without lowering the incidence energy for the reaction onset, thus reducing the slope of the sticking curve. To test this, we present quasi-classical trajectory (QCT) calculations on the O₂ + Al(111) system based on a potential energy surface (PES) computed with the HSE06-1/2x-VdWDF2 screened hybrid van der Waals DF, using the Born-Oppenheimer static surface (BOSS) model. The resulting PES shows the presence of shallow van der Waals wells in the entrance channel. Furthermore, the barriers to DC show a slightly higher energetic corrugation than the previously used HSE03-1/3x screened hybrid DF, although most differences are smaller than 1 kcal/mol. These minor alterations in the PES with respect to previous work mean that the S_0 computed for $O_2 + Al(111)$ using the HSE06-1/2x-VdWDF2 DF are somewhat improved over the previous results. Specifically, the onset of the S_0 curve is now somewhat better described and the curve is broadened a little compared to the HSE03-1/3x description. These results, in combination with previous studies, imply that future electronic structure methods would need to provide larger changes in the PES, or a different dynamical model would need to be used to bring theory in better agreement with the experiment. Moreover, future higher-level theory also needs to address the currently very demanding computational costs of screened hybrid plane-wave-DFT for molecule-metal interactions.

1. INTRODUCTION

The rate of heterogeneously catalyzed processes is often controlled by the dissociative chemisorption (DC) of a molecule on the active center of the catalyst. 1-3 Furthermore, for oxidative catalysis or oxide formation, the DC of O2 is often the first and most critical step. 4-7 The key interactions that are at play in the DC of O₂ on metals are not yet fully understood⁸⁻¹⁰ and are therefore of substantial scientific interest. $^{11-14}$ The O₂ + Al(111) system has over the years become a benchmark for the DC of O_2 on metal systems. However, unlike the perhaps better-known H_2 + Cu(111) benchmark system, O_2 system, theoretical models are not yet able to describe the DC of O2 on Al within chemical accuracy, 10 nor is there a clear scientific

consensus on the origins of the barrier to DC for this system.^{8,9,23–28}

Both the failure of theoretical models to describe the DC of O_2 on Al(111) and the ongoing discussion on the origin of the barrier to reaction can be related to the inability of the most

Received: January 15, 2025 Revised: February 19, 2025 Accepted: February 21, 2025

Published: March 6, 2025





commonly applied density functional theory (DFT) method in surface science to compute the DC barrier. $^{8-10,23,24,27-32}$ The generalized gradient approximation (GGA) approach to the density functional (DF) remains the most commonly used approach to compute reaction barriers 14 within surface science because it represents a good compromise between accuracy and computational costs. However, recent work 10 strongly suggests that the GGA approach will fail to compute accurate reaction barriers if the charge transfer energy ($E_{\rm CT}$) is below 7 eV, where $E_{\rm CT}$ is defined as

$$E_{\rm CT} = \phi - EA \tag{1}$$

Here ϕ is the work function of the metal surface, and EA is the electron affinity of the molecule reacting on that surface. 10 If $E_{\rm CT}$ is below 7 eV even one of the most "repulsive" (i.e., a "more repulsive DF" is a DF generally predicting higher DC barriers) GGA DFs (i.e., RPBE 33) tends to underestimate the barrier height to DC. 13,14,34,35 This means that, when constructing a chemically accurate semiempirical DF using the specific reaction parameter approach, i.e., an SRP DF, basing this DF on GGA DFs will probably not be possible. 10,34 For O $_2$ + Al(111) $E_{\rm CT}$ = 3.8 eV 10 , and all GGA DFs fail to compute any relevant barrier. This in turn results in computed reaction probabilities that are always equal or close to one and thereby in disagreement with the experiment, which shows activated dissociation for O $_2$ on Al(111). $^{10,30-32}$ Likewise, meta-GGA DFs, which are on the next rung up on Jacob's ladder, 36 show only a minor improvement over GGA results for O $_2$ + Al(111). 10

At this time it is not fully understood why $E_{\rm CT}$ < 7 eV results in a failure of DFs containing semilocal exchange for DC on metals. The failure of GGA DFs to accurately predict barriers for molecule-metal reactions may be related to the more general failure of GGA DFs to predict barriers for gas-phase reactions, as also previously discussed by Gerrits et al.¹⁰ The commonly applied reasoning is that GGA DFs favor the delocalized nature of a transition state (TS) and thus result in TS-energies that are too low compared to the reactants, resulting in too low or even eliminating the barriers. For gas-phase reactions such a "densitydriven" error could then be and has been resolved by using semilocal DFs in a nonself-consistent-field (NSCF) manner by applying a GGA-DF once to a converged density obtained with a hybrid DF, i.e., a "HF-based density", where HF stands for Hartree–Fock. 37-40 However, the explanation that this approach yields more accurate barriers due to correcting for density-driven errors has come under scrutiny as recent work indicates that the improved agreement is due to a cancellation between both density-driven and "functional-driven" errors. 41,42 Moreover, the explanation in terms of only density-driven errors is also at odds with previous results for $O_2 + Al(111)$, which showed that good sticking probabilities can be computed with both SCF- and NSCF-screened hybrid approaches, where in the latter a screened hybrid DF is applied just once to a converged GGA density. This implies that the greater part of the GGA-DFT error for O_2 + Al(111) should be functional-driven. ^{37,38,43}

Regardless of the origin of the error of the semilocal exchange DF, previous work suggests that the failure of these types of DFs for $O_2 + Al(111)$ should be avoided by employing a screened hybrid DF instead. The use of the screened hybrid HSE03-1/3x DF resulted in reaction probabilities that were in semiquantitative agreement with the experiments. Especially the reaction probabilities at lower normal incidence energy (E_I^{-1}) closely reproduce experimental results. 10,43,44 However, at higher E_I^{-1} the computed sticking probabilities still overestimate

the experimentally determined sticking probabilities. This resulted in a reaction probability curve that is too steep, or too narrow. 10,43 To find a DF that can reproduce experiments with chemical accuracy for systems like $\rm O_2 + Al(111)$, this problem still needs to be fixed.

Several alternative possibilities could contribute to a toonarrow reaction probability curve. The first few are due to the use of the Born-Oppenheimer static surface (BOSS) model. In the Born-Oppenheimer approximation, the electronic energy is decoupled from nuclear motion, and in the static surface approximation, the surface atoms of the metal are kept fixed in their ideal surface lattice positions. Because experiments indicate a limited influence of surface temperature on the reaction probability of O₂ on Al(111),¹⁷ it is not immediately expected that the inclusion of surface phonon motion will substantially influence the reactivity. ^{10,17,43} Furthermore, if the barrier location as described by the HSE03-1/3x DF is to be taken as accurate, which is likely according to previous work,³⁴ then the $O_2 + Al(111)$ system will generally have "early" barriers, i.e., the barriers will be located at large molecule—surface distances. 9,10,23,24,43,44 Such early barriers tend to limit the effects of energy dissipation from the motion of the molecule to surface atom motion. 10,45,46 Furthermore, the early barrier and the high mass of O2 also suggest that the effects of electron-hole pair (ehp) excitation, which can be described with electronic friction approaches, should be small. 47-49 This likely also eliminates the effects of ehp excitation as a possible important cause for the disagreement between theory and experiments for O2 +

If we assume that the BOSS model is not to blame for the currently deficient theoretical description of the DC of O2 on Al(111), only the electronic structure description remains a likely cause of error, as also previously argued in refs 10 and 43 As stated above it was expected that the inclusion of long-range van der Waals (VdW) correlation in the exchange—correlation functional could result in a broadening of the reaction probability curve, but this has so far not yet been corroborated. This hypothesis is supported by the argument that the introduction of a VdW well will increase both the energetic and geometric corrugation of the barrier. 50 The energetic corrugation is the extent to which the barrier height varies with the impact point of the surface and the orientation of the molecule and this strongly influences the width of the reaction probability curve. 35,51 Additionally, a VdW well could alter the dynamics of O2 impeding on the surface by accelerating the molecule toward the metal surface before dissociation.⁵

In this work, we aim to investigate the simultaneous effects of the inclusion of VdW correlation and of admixing a larger amount of exact exchange on the potential energy surface (PES) as well as the dynamics of the DC of O_2 on Al(111), by computing and analyzing a PES based on the HSE06-1/2x-VdWDF2 DF and comparing quasi-classical trajectory (QCT) dynamics results based on this PES to experiments and previous theoretical studies. The aim of applying this DF is to hopefully resolve the current shortcomings in the description of the DC of O_2 + Al(111). This paper is set up as follows: Section 2.1 will discuss the details of the DF used to compute the electronic structure, Section 2.2 the computational details of the DFT calculations, Section 2.3 the Al(111) lattice details, Section 2.4 the PES fitting technique, and Section 2.5 the QCT calculations. Thereafter, the DFT results are shown in Section 3.1, and in Section 3.2 the QCT dynamics results are shown. Section 3.3 then discusses the results in the context of previous work and

presents an outlook for future work. Finally, the paper is summarized and conclusions are provided in Section 4.

2. METHODS

In this work, the Born–Oppenheimer static surface (BOSS) model is employed. ¹⁴ In short, this signifies that the motion of the nuclei is decoupled from the motion of the electron via the Born–Oppenheimer approximation, and that the Al surface atoms are kept static in their ideal (111) surface lattice positions. As a result, the dynamics of the O_2 on the Al(111) system only requires a description of the motion in the remaining six molecular degrees of freedom. These six degrees of freedom in addition to a description of the high symmetry sites on the Al(111) surface are shown in Figure 1 and discussed in greater detail in other work. ^{10,13,43}

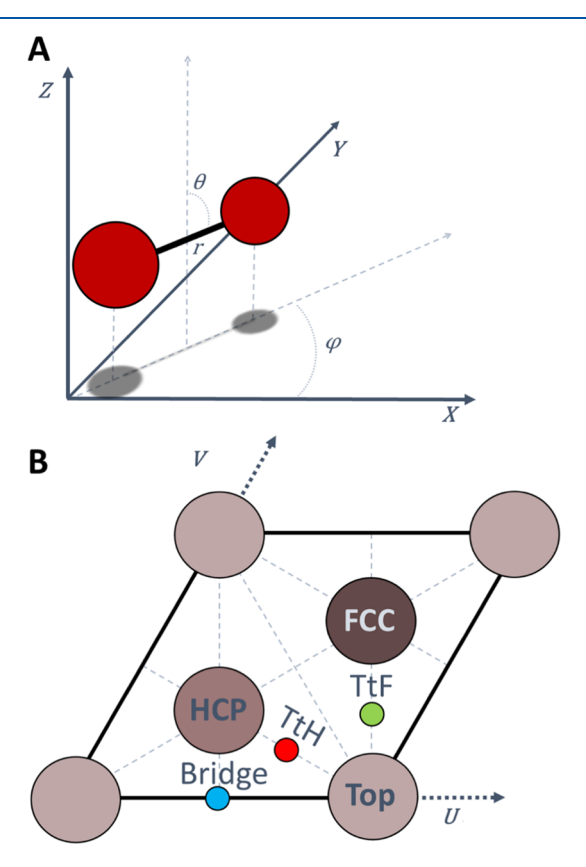


Figure 1. Coordinate system and its relation to the Al(111) unit cell; (A): six-dimensional center-of-mass coordinate system for the O_2 molecule; (B): (111) surface unit cell for an FCC metal (Al) with all high symmetry sites indicated. A darker shade represents an atom that is in a deeper layer in the slab.

2.1. Electronic Structure. For this paper, a combination of two different types of DFs is used to improve the description of the electronic structure. Specifically, the nonlocal van der Waals-DF2 (VdWDF2)^{S3,S4} correlation functional and the screened exact exchange DF of the HSE06^{S5,S6} DF are combined. Below we will briefly discuss these DFs, first as standalone DFs and then quickly as their combination.

Local or semilocal DFs will inherently not be able to describe the longer-range electronic correlation necessary to accurately describe effects like VdW forces. Several different approaches have been developed to correct the long-range correlation of the exchange—correlation functional for such shortcomings. For instance, approaches that use a pairwise potential based on time-dependent DFT to include VdW interaction have been developed by Grimme and co-workers. This is Initial work of Lundqvist et al., forms the basis for multiple different VdW methods better suited for metal-molecule interactions, like the VV10, VV10, VdWDF1, and VdWDF2, DFs. Of these DFs VdWDF1 represents a truly nonempirical DF., i.e., this method is not based on fitted adjustable parameters.

In this work we use the VdWDF2⁵⁴ approach, in which a nonlocal (NL) longer-range correlation energy is added to a local (LDA) correlation energy, resulting in the following expression for the correlation functional

$$E_{\rm C}^{\rm VdWDF2} = E_{\rm C}^{\rm LDA} + E_{\rm C}^{\rm NL, VdWDF2}$$
 (2)

Note that an exchange DF (E_x) can be added to this DF that can be local, semilocal or even a nonlocal DF including exact exchange. The van der Waals correction to the correlation energy can be written as

$$E_{\rm C}^{\rm NL,VdWDF2} = \int d\vec{r} \int d\vec{r}' n(\vec{r}) \phi(\vec{r}, \vec{r}') n(\vec{r}')$$
(3)

Here \vec{r} is the position vector of the electrons, $n(\vec{r})$ the electronic density, and $\phi(\vec{r}, \vec{r}')$ the van der Waals kernel describing the electron density—density interactions. A full discussion of this kernel is out of scope for this work and the reader is referred to refs 53 and 54 for more details.

The effects of the VdWDF2 correlation on the PES are not known a priori, although its addition will generally improve the description of longer-range interactions and improves over PBE in describing the adsorption of molecules on metals. 14,62 The presumption is that a longer-range attraction, i.e., a van der Waals well will form in the PES, 63 although it is not uncommon for the middle—range interaction to become slightly more repulsive. 52 As the barriers for $\rm O_2$ on Al(111) are far away from the surface, it is expected that the use of VdW correlation will tend to reduce the barrier height. 10

Moving on to the screened hybrid exchange functional, we use the HSE06 56 DF. This DF is very similar to the HSE03 DF 56 , the expression of which was later revised to obtain the HSE06 DF. 57 The HSE06 DF is a hybrid DF because a fraction (α) of exact (Hartree–Fock) exchange is admixed with the semilocal PBE 64 exchange–correlation functional according to

$$E_{\rm XC}^{\rm PBE0} = \alpha E_{\rm X}^{\rm HF} + (1 - \alpha) E_{\rm X}^{\rm PBE} + E_{\rm C}^{\rm PBE}$$
 (4)

This makes the HSE06 DF similar to the better-known PBE0⁶⁵ DF. However, unlike the PBE0 DF, the HSE06 DF also screens the exact exchange at longer electron–electron distances. As a result, at short distances, the DF behaves like PBE0 but at longer distances like PBE. This screening is done with a continuous and quick switching function between a longrange (LR) and short-range(SR) part in the Hartree–Fock (HF) exchange potential, such that the coulomb operator splits into

$$\frac{1}{r_{ij}} = \frac{1 - \operatorname{erf}(\omega, r_{ij})}{r_{ij}} + \frac{\operatorname{erf}(\omega, r_{ij})}{r_{ij}}$$

$$= \frac{r_{ij}}{\operatorname{LR}}$$
(5)

where r_{ij} is the distance between electrons i and j, $\text{erf}(\omega, r_{ij})$ is the Gaussian error function, and ω is the screening length parameter. The result of this adaptation of the HF exchange potential is that the HSE06 exchange—correlation functional can also be partitioned into a short and long-range part, such that

Table 1. Comparing Al(111) Surface Layer Expansion and Contractions of This Work with Experiments and Other Theories

	LEED experiments on 160 K ⁸⁶	$HSE03-1/3x^{10}$	LDA ⁸⁷	HSE06-1/2x-VdWDF2 (this work)
d_{12}	$1.7\% \pm 0.3\%$	1.4%	1.18%	1.83%
d_{23}	$0.5\% \pm 0.7\%$		-0.40%	-1.16%
d_{34}			0.22%	

$$E_{\text{XC}}^{\text{HSE06}} = \alpha E_{\text{X}}^{\text{HF,SR}}(\omega) + (1 - \alpha) E_{\text{X}}^{\text{PBE,SR}}(\omega) + E_{\text{C}}^{\text{PBE,LR}}(\omega) + E_{\text{C}}^{\text{PBE}}$$
(6)

The screening of the HF exchange for longer distances is needed to reduce computational costs, ⁵⁵ and the screening is required to obtain a good description of the metal surface itself. Without it, the density of states of the electrons at the Fermi level would be artificially reduced. ⁶⁶

The implementation of the screened hybrid exchange functional in this work has an important difference from that of the original HSE06 DF: ⁵⁷ In this work, we use a larger fraction of exact exchange. Originally, the HSE06 DF comes with a maximum exact exchange fraction α of 1/4. Previous work with an HSE03-like DF used $\alpha = 1/3^{10}$ but still resulted in overestimated sticking probabilities, suggesting that α should be increased further. In this work, we therefore opted to use an exact exchange fraction α of 1/2. Increasing the fraction of exact exchange is a common approach to improve the performance of the DF for gas-phase barriers by increasing the barrier height.^{67–69} An exact exchange fraction of 1/2 could also result in an overestimation of the barrier height, ⁶⁹ as it did in similar work on O_2 + Cu(111).⁷⁰ However, at the outset, we realized that we might need to compensate for a barrier-lowering effect by replacing the PBE correlation with the van der Waals correlation, 10,63 as also discussed above, and for this, an increased fraction of exact exchange over the previously used value of 1/3 was deemed necessary.

The combination of both the screened hybrid exchange and the van der Waals correlation DF results in the HSE06-1/2x-VdWDF2 DF

$$E_{\text{XC}}^{\text{HSE06-VdWDF2}} = \frac{1}{2} E_{\text{X}}^{\text{HF,SR}}(\omega) + \frac{1}{2} E_{\text{X}}^{\text{PBE,SR}}(\omega) + E_{\text{X}}^{\text{VdWDF2}}$$

$$+ E_{\text{X}}^{\text{PBE,LR}}(\omega) + E_{\text{C}}^{\text{VdWDF2}}$$
(7)

It is expected that the HSE06-1/2x-VdWDF2 DF will adequately describe longer-range interactions and thereby result in the presence of a VdW well in the entrance channel, while hopefully also still correctly describing the barrier height. In previous work, the DF defined by eq 7 was tested as the first hybrid-VdW DF to yield dynamics results for the DC of O₂ on Cu(111). For that system the DF tended to underestimate the reaction probability, i.e., it overestimated the barrier heights.⁷⁰ Although for O_2 + Cu(111) this was the first DFT result to ever underestimate sticking, we do not expect that the HSE06-1/2x-VdWDF2 would also result in an underestimated sticking probability for the O_2 + Al(111) system based on the previous results obtained with $\alpha = 1/3$, 10,43 and on $O_2 + Al(111)$ having only a single barrier to reaction in the entrance channel, unlike the O_2 + Cu(111) system which also has a second barrier in the exit channel.

Lastly, it is important to differentiate the HSE06-1/2x-VdWDF2 DF from screened hybrid VdW DFs where the exchange part of the DF is not tailored to or made consistent with the van der Waals correlation functional, e.g., VdW-DF2-ahbr. The HSE06-1/2x-VdWDF2 DF does not represent a

completely new screened hybrid VdW DF, as provided by the recent work of Hyldgaard and co-workers. ^{71,72} Instead, our DF is simply a combination of two established exchange and correlation DFs, as described above.

2.2. Computational Details. Als DFT calculations are done with the Vienna Ab Initio Simulation Package (VASP) version 6.3.2^{73–78} using the van der Waals DFT implementation of Klimeš et al. ^{79,80} In this work, all energies from the HSE06-1/2x-VdWDF2 DF are based on three distinct successive self-consistent-field (SCF) single-point calculations. The computational costs of converging the electronic structure energy with the HSE06-12/x-VdWDF2 DF from scratch are high. Therefore, two precalculations, or "primers", have been performed to set up initial guesses for the electronic density and Kohn—Sham (KS) wave function. The first SCF primer uses the PBE-VdWDF2 DF, the second SCF calculation the HSE06-1/2x-VdWDF2 DF with a sparse HF integration grid, and the third and final SCF single point calculation uses a normal HF integration grid to improve accuracy.

All three SCF calculations, that is the two primers and the final SCF calculation, are spin-polarized calculations and use a 2×2 4-layer Al supercell (see the next section for the lattice details) with 15.0 Å vacuum above the slab. All three use a $10 \times 10 \times 1$ Γ centered k-point grid and a cutoff energy of 400 eV. The core electrons of both Al and O are described by the projector augmented wave (PAW)81 method, as developed for the PBE DF. Methfessel-Paxton smearing with a width of 0.2 eV is used to improve convergence. The PBE-VdWDF2 primer uses the "conjugate" algorithm 82,83 with a convergence tolerance of 1.0 \times 10⁻⁹ eV, as done in previous work. 43,70 After this primer is finished, its electron density and KS-wave function are used for the next primer with the HSE06-1/2x-VdWDF2 DF, using the damped algorithm, as without this algorithm numeric stability is limited, and a convergence criteria of 1.0×10^{-5} eV, or a limit of 240 SCF steps is used. Furthermore, the "Fast", i.e., sparse HF integration grid is employed.⁸⁴ This final primer single-point calculation will, if all goes well, usually consume the bulk of the computational time. After this, another HSE06-1/2x-VdWDF2 single-point calculation is started using the previous KS-wave function with a normal HF integration grid to improve the accuracy of the final result. This final SCF single point is then converged to 1.0×10^{-5} eV again. Converged results were obtained for all but one data point (U = 0, V = 0, $\theta = 90^{\circ}$, $\varphi =$ 30° , Z = 4.0 Å, r = 1.175 Å), the energy of which was interpolated based on surrounding data points. Despite the use of these tricks, the computational demands for this project are still large: we have consumed upward of 30 million CPU hours for this PES, where a single point typically takes a minimum of 1 week but can easily take 2 weeks or longer on a modern dual socket AMD EPYC 7351 32 core node, depending on the difficulty of the convergence.

2.3. Lattice Details. The Al bulk lattice has been relaxed using the HSE06-1/2x-VdWDF2 DF, using a 1 × 1 × 1 bulk supercell with 11 × 11 × 11 Γ -centered k-points, while maintaining the other computational settings as described above. The lattice constant is relaxed at 4.041 Å. This is in good

agreement with the experimental lattice constant of 4.032 Å. The surface lattice structure was then further relaxed using a 1 \times 1, 4-layer supercell with the bottom 2 layers frozen and 15 Å of vacuum using a 20 \times 20 \times 1 Γ -centered k-point grid. This resulted in interlayer distances of $d_{12}=2.376$, $d_{23}=2.306$, with $d_{34}=2.333$. Table 1 presents comparisons of this lattice expansion/contraction to other works, which shows that the top layer expansion is in good agreement with experimental and other theoretical work. To maintain consistency with the 2 \times 2 unit cell the number of k-points parallel to the Al surface is halved for the PES production, see the computational details above.

2.4. Fitting the PES. The interaction of $O_2 + A(111)$ is described with a continuous six-dimensional (6D) PES that is interpolated from the electronic structure calculations performed with the above-described HSE06-1/2x-VdWDF2 density functional. To obtain a good interpolation quality the corrugation reduction procedure $(CRP)^{88,89}$ is used. In this procedure, two three-dimensional (3D), or atomic, PESs are subtracted from the 6D diatomic PES. This is done to obtain a residual PES with reduced corrugation, which is easier to interpolate accurately. After this, the 3D PESs are added back to the full interpolated result. The resulting error of the CRP for predicting energies of points not part of the interpolation grid used to obtain the PES should be minor: 43,89-91 previous work using the same (U, V, θ, φ) geometries and comparably fine grids in r and Z has shown an RMSE of 0.8 kJ/mol (0.2 kcal/mol) as long as interaction energies of the molecule with the metal are smaller than 4 eV⁹¹, with outlier usually below 3 kJ/mol. 43,89,91 The CRP as implemented in this work is similar to that of refs 10, 43 and 92 However, a few distinctions will be highlighted below.

First, the atomic PES is not based on the HSE06-1/2x-VdWDF2 DF but on the PBE-VdWDF2 DF. This is done to mitigate the computational cost. Additionally, the atomic PES is based on spin unpolarised DFT, unlike the 6D molecular PES. This avoids convergence issues as the open-shell nature of an O atom results in significant noise in the DFT energies far away from the Al surface. Computing the 3D atomic PES with spinunpolarised DFT does not affect the accuracy of the full 6D PES as subtracting the 3D atomic PESs from the full 6D PES merely serves to yield a 6D residual term with decreased corrugation and anisotropy. Adding the 3D atomic correction terms back on to the residual PES then yields the spin-polarized 6D DFT data at the points used for interpolation. Furthermore, the convergence criteria are slightly lighter than in the primer calculations, as discussed in Section 2.2, and are set to 1.0×10^{-8} eV. These nuances are possible because the atomic PES does not need to be very accurate as long as it is physically reasonable, as also discussed in refs 10, 43 and 70 For instance, by using the cheaper to evaluate PBE-VdWDF2 DF we ensure that the longrange interactions are described. As a result, one or 2 orders of magnitude in computational costs can be saved for the atomic potential. The *U*, *V* grid for this 3D atomic PES is similar to that used in earlier CRP work, 10,43,92 and the Z-Grid is an equidistant grid between -1.20 and 8.50 Å with a 0.05 Å spacing, leading to a total of 194 grid points for each of the 10 different surface sites.

Second, the 6D PES grid is not equidistant as in ref 92 Instead a similar grid structure as in refs 10 and 43 is used but extended to allow for longer-range interactions captured by the addition of the VdW-DF2 DF. Thus, this results in the grid: $Z = \begin{bmatrix} 1.00, 1.50, 2.00, 2.25, 2.50, 2.75, 3.00, 3.25, 3.50, 3.75, 4.00, 4.25, 4.50, 4.75, 5.00 \end{bmatrix}$ Å, and $r = \begin{bmatrix} 1.000, 1.100, 1.150, 1.175, 1.190, 1.200, 1.225, 1.250, 1.300, 1.400, 1.500, 1.600 \end{bmatrix}$ Å. To clarify this point further,

these Z and r grids are used for each U, V, θ , and φ geometry employed, and the values of the coordinates of the relevant geometries are shown in Table 2. The PES in the gas phase is

Table 2. Different Combinations of the U, V, θ , and φ Coordinates That are Used in the Grid to Interpolate the PES^a

site name	U	V	$[heta, oldsymbol{arphi}]$
top	0	0	[0, 0], [90, 0], [90, 30]
bridge	1/2	0	[0, 0], [90, 0], [90, 60], [90, 90]
HCP	1/3	1/3	[0, 0], [45, 30], [45, 210], [90, 0], [90, 30]
TtH	1/6	1/6	[0, 0], [45, 30], [45, 120], [45, 210], [90, 30], [90, 120]
TtF	1/3	-1/6	[0, 0], [45, 150], [45, 240], [45, 330], [90, 240], [90, 330]
FCC	2/3	-1/3	[0, 0], [45, 150], [45, 330], [90, 0], [90, 330]
a			

^aThe *U* and *V* coordinates are shown in Figure 1.

extrapolated beyond 5.00 Å up to 7.50 Å via a switching function to a 2D potential, similar to previous work. This grid spacing limits the total number of required single points while maintaining enough details near the transition state and in the gas-phase to properly describe both the dissociative chemisorption and the van der Waals interaction. All in all, this makes for a total of 5260 different single points used to interpolate the PES.

2.5. Quasi-Classical Trajectory Dynamics. The continuous 6D CRP-PES can be used to compute the reaction probabilities of $\rm O_2$ on Al(111) with dynamics calculation using the quasi-classical trajectory (QCT) method. $\rm ^{93,94}$ QCT calculations include the zero-point energy of the molecule through the initial conditions imposed, after which the equations of motion are propagated classically in time. $\rm ^{93,94}$ The molecule is initially placed at 7.00 Å above the surface with a given incidence energy, with its velocity vector pointing along the surface normal. The trajectory is counted as reacted if the $\rm O_2$ bond length exceeds 1.59 Å, or it is considered scattered if the molecule—surface distance exceeds 7.00 Å and the velocity of the molecule points away from the Al surface. The reaction probability is then calculated as

$$P_r = \frac{N_r}{N_T} \tag{8}$$

where N_T is the total number of trajectories, and N_r the number of trajectories that reacted. See refs 10, 90 and 95 for further details on the implementation of the QCT dynamics.

To assess the quality of the DF, computed sticking probabilities need to be compared to King and Wells experiments. 13,14,96 In this work, we compare with the supersonic molecular beam experiments of Österlund et al. 17 The experimentalist varied the nozzle temperature $(T_{\rm N})$ and used seeding in He and antiseeding in Xe to vary the $E_{\rm I}^{-1}$. For the sticking curve that we aim to reproduce the authors stated that all O_2 molecules were in the vibrational ground state. However, no time-of-flight measurements are available for this study. Moreover, previous theoretical studies used a $T_{\rm N}=300~{\rm K}$, 10,43 thus, to fairly compare the effect of the incidence energy on the DC of O_2 we computed the reaction probabilities as a function of single $E_{\rm I}^{-1}$ values with the vibrational temperature of O_2 taken to be the same as in previous work, i.e., $300~{\rm K}$. 10,43 To describe the effect of the high rotational cooling of O_2 the rotational

temperature is simply taken as having a single value of 9 K; ⁹⁷ this represents an approximation. In the QCT of this work, we have allowed the states v = 0-3 and j = 1-49 to get occupied. This results in an 80% occupation of the rovibrational ground state: v = 0, j = 1, see refs 90 and 98 for more information. Note that even j states are forbidden via nuclear spin statistics for O_2 in the electronic ground state. The Supporting Information of ref 43 provides a breakdown of all the occupied initial states. To compute the reaction probabilities (P_r) with converged statistics we ran at least 10^5 trajectories per E_1^{\perp} .

3. RESULTS AND DISCUSSION

Below the results will be discussed in three distinct sections. In the first section, the effects of the DF on the electronic structure description and potential energy surface are discussed. The second section discusses the QCT results and compares them to previous work. Lastly, the impact of the new HSE06-1/2x-VdWDF2 DF is discussed in the context of the literature and what these results mean for future descriptions of this system.

3.1. Potential Energy Surface and Barrier Analysis. Before discussing the new QCT dynamics results, it may be insightful to discuss the effects of the VdW correlation and the increased exact exchange fraction of the HSE06-1/2x-VdWDF2 DF on the electronic structure of the O₂ + Al(111) system, and the resulting changes of the PES compared to previous electronic structure calculations with $\alpha = 1/3$ and using PBE correlation. ^{10,43,44}

The most immediate and important change is the consistent presence of a VdW well. This well appears in the entrance channel, i.e., at larger molecule—surface distances than where the barrier to dissociation is found, at about 3.5 Å above the Al(111) surface. In Figure 2 a selection of potential curves

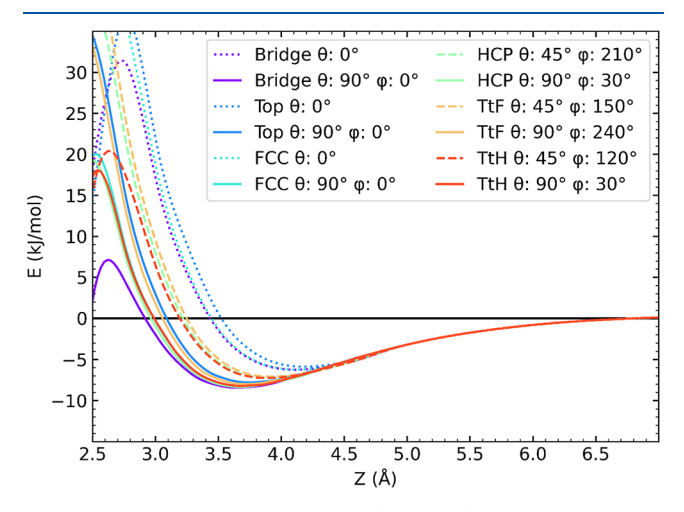


Figure 2. Electronic potential energy (in kJ/mol) as a function of the molecule surface-distance Z for a fixed O_2 bond length of 1.19 Å at different U, V impact sites and for different molecular orientations (see also Figure 1).

including VdW wells are plotted as a function of the molecule—surface distance (Z) for O₂ at a constant bond length r=1.19 Å. The PES cuts shown in Figure 2 differ in the surface site (U, V) and O₂ orientation given by θ and φ . Figure 2 shows that the VdW well appears to be almost completely independent of the O₂ adsorption site and φ . However, the depth and location in Z of the well do depend on θ : The well-depth depends on whether the molecule is orientated parallel or normal to the surface. The

well tends to be shallowest and furthest away from the surface for $\rm O_2$ orientated normal to the surface, and deepest and closest to the surface for the planar orientation. These results are reminiscent of the VdW wells that are computed for $\rm O_2$ + $\rm Cu(111)$ with the same HSE06-1/2x-VdW DF as used here. ⁷⁰

Unlike the surface site independence of the VdW well, Figure 2 also shows a glimpse of a different dependence effect, i.e., a strong dependence of the barrier height on the impact site of the molecule. Although the bond length is kept constant in Figure 2 the results obtained at lower Z values strongly suggest that the barriers vary greatly depending on the O2 geometries. The actual barriers to dissociation occur at slightly elongated bond lengths as also found earlier. 43 The actual barrier heights are presented in Table 3. This table also compares the barrier heights obtained with the HSE03-1/3x DF^{10} and the nonself-consistent field (NSCF) approach implemented through the HSE03-1/3x@ RPBE DF, which amounts to obtaining the electronic energy through a single application of the HSE03-1/3x DF to a converged RPBE density. 43 Furthermore, the left column of the table is bold or italics depending on the relative difference of barrier heights between the results of the HSE06-1/2x-VdWDF2 DF and the HSE03-1/3x DF to aid the reader in judging the shifts in barrier heights.

The results presented in Table 3 are also shown in the form of a bar plot in Figure S1 of the Supporting Information. Both Table 3 and Figure S1 show that the barrier heights to DC computed with the HSE06-1/2x-VdWDF2 are not very different from the values computed with the HSE03-1/3x DF: the majority of the barrier heights are within $\pm 1 \text{ kcal/mol}$ ($\approx 4.2 \text{ kJ/mol}$ mol), of one another. This is true except for three configurations in which O₂ is oriented normal to the surface and impinges on an HCP, FCC, or TtH site. The barrier heights at these geometries differ by more than 1 kcal/mol. Another noteworthy element is that the difference in barriers does not seem to follow any clear trend, i.e., some barriers are lower when computed with the HSE06-1/2x-VdWDF2 DF but most are slightly higher in energy. The overall effect is that the energy range over which the barriers are spread is increased slightly when employing the HSE06-1/2x-VdWDF2 DF, or, put differently, the energetic corrugation of the barrier is increased meaning that the barrier height varies more strongly with impact site and orientation of the molecule.

The increased energetic corrugation may result in a slight broadening of the sticking probability curve. This is what was both desired and expected from the use of the screened hybrid van der Waals DF. However, we should note that the effect on the barriers by switching DFs is small. As discussed above, most barriers are within 1 kcal/mol of the old results and thus the effectiveness of this increased energetic corrugation may be limited. Furthermore, Table 3 also shows the barrier heights as computed with the NSCF HSE03-1/3x@RPBE DF. 43 Switching to the NSCF approach only results in higher barriers than obtained with the SCF HSE03-1/3x DF, but generally seems to increase the energetic corrugation of the barrier more than switching to the HSE06-1/2x-VdWDF2 DF does. The differences between the sticking curves computed based on the NSCF and SCF HSE03-1/3x DFs were minor 43 and thus, the effectiveness of increasing the barrier corrugation and anisotropy by the use of the HSE06-1/2x-VdWDF2 may be expected to be limited. This concern was also raised in previous work. Thus, the effectiveness of changing to the HSE06-1/2x-VdWDF2 DF might be smaller than we had hoped for unless,

Table 3. Barrier Heights (in kJ/mol) Computed for Specific U, V, θ, φ Geometries for O₂ + Al(111) with the HSE06-1/2x-VdWDF2 DF, the HSE03-1/3x DF, ¹⁰ and the NSCF HSE03-1/3x@RPBE DF⁴³

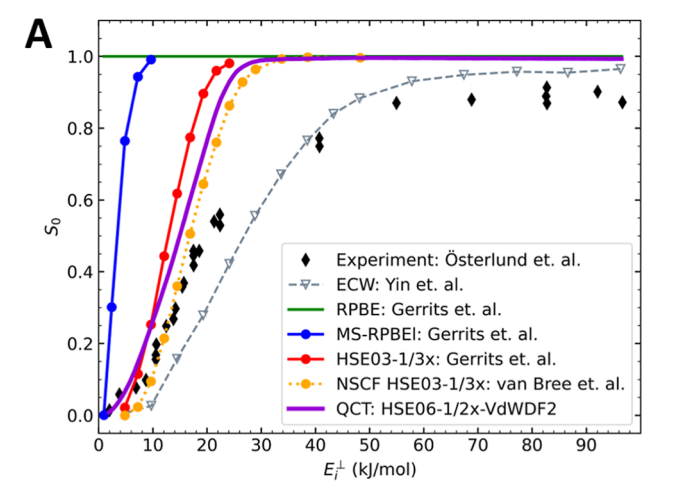
location ^a	HSE06-1/2x- VdWDF2 (kJ/ mol)	HSE03-1/3x (kJ/mol)	HSE03-1/3x@ RPBE (kJ/mol)
TtF θ : 0°	26.7	22.9	29.1
TtF θ : 45 φ : 150 $^{\circ}$	25.4	26.1	38.0
TtF θ : 45 φ : 240°	13.4	12.5	16.7
TtF θ : 45 φ : 330°	15.9	14.4	16.6
TtF θ : 90 φ : 240°	26.4	23.6	28.7
TtF θ : 90 φ : 330°	9.9	10.7	12.8
TtH θ: 0°	26.1	21.9	27.7
TtH θ : 45 φ : 120°	14.1	12.8	16.9
$TtH \theta$: 45 φ : 210°	24.9	25.3	36.3
TtH θ : 45 φ : 30°	15.9	14.4	16.8
TtH θ : 90 φ : 120°	25.8	23.7	37.9
$TtH \theta$: 90 φ : 30 $^{\circ}$	9.3	10.1	12.3
FCC θ : 0°	34.4	26.9	38.5
FCC θ : 45 φ : 150°	25.0	24.6	32.5
FCC θ : 45 φ : 330 $^{\circ}$	39.1	39.9**	60.0**
FCC θ : 90 φ : 0 $^{\circ}$	11.0	11.5	13.5
FCC θ : 90 φ : 330°	12.4	12.4	14.6
bridge θ: 0°	23.0	19.5	25.5
bridge θ : 90 φ : 0°	2.0*	4.7*	6.6*
bridge θ : 90 φ : 60°	21.0	19.6	29.7
bridge θ : 90 φ : 90°	30.7	29.5	51.4
HCP θ: 0°	28.6	22.8	34.6
HCP θ : 45 φ : 210°	23.9	23.3	31.0
HCP θ : 45 φ : 30 $^{\circ}$	39.2**	39.9**	56.2
HCP θ : 90 φ : 0 $^{\circ}$	9.8	10.4	12.7
HCP θ : 90 φ : 30 $^{\circ}$	11.2	11.4	13.7
top θ: 0°	30.9	26.8	29.8
top θ: 90 φ: 0°	25.4	22.7	24.4
top θ : 90 φ : 30°	25.2	22.5	24.4

^aThe format of the barrier location cell indicates the difference in the barrier height computed with the HSE06-1/2x-VDWDF2 DF and the HSE03-1/3x DF. **Bold** indicates a higher barrier energy for the HSE06-1/2x-VdWDF2 DF and *italics* lower energy. An asterisk (*) indicates a larger effect. Distinctions are made, i.e., binned per 1/2 kcal/mol (\approx 2 kJ/mol). For each DF the lowest and highest values of the barrier height computed with the DF are indicated with * and **, respectively.

e.g., the presence of the VdW well would substantially alter the nature of the dynamics.

3.2. Quasi-Classical Trajectory Results. The QCT dynamics calculations were performed for 491 different normal incidence energies varying from 0.020 to 1.000 eV with steps of 0.002 eV. For every incidence energy, a total of 10^5 trajectories were simulated using a maximum propagation time of 1 ns. The resulting sticking probabilities (S_0) are presented in purple in Figure 3. The experimental S_0 and the S_0 computed by other theories are also presented as a comparison.

The onset of S_0 for the HSE06-1/2x-VdWDF2 DF is best seen in the log plot of Figure 3B and shows that some reaction already occurs at $E_1^{\perp} = 2$ kJ/mol. The reactivity then quickly increases to



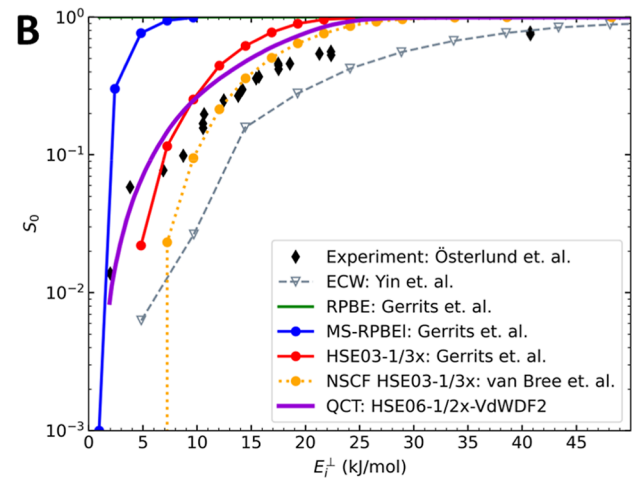


Figure 3. Sticking probabilities as a function of normal incidence energy; (A): normal *y*-axis; (B): Log *y*-axis, and shorter range of the *x*-axis, for clarity. Plotted are the sticking probabilities of the experiments (black diamonds) by Österlund et al., ¹⁷ ECW results of Yin et al. ²⁴ (gray dashed line), results using the RPBE DF (green solid line), MS-RPBEI DF (blue solid line), and the HSE03-1/3*x* DF (red solid line) of Gerrits et al., ¹⁰ the NSCF HSE03-1/3@RPBE DF (orange dotted line) of van Bree et al., ⁴³ and the HSE06-1/2*x*-VdWDF2 DF (this work, purple solid line)

1 over the range of 2–32 kJ/mol, as seen in both Figure 3A,B. For higher $E_{\rm I}^{\ \perp}$ the S_0 remains constant around 1, although a maximum of 0.996 is found at $E_{\rm I}^{\ \perp} \approx 57$ kJ/mol after which S_0 seems to consistently drop slowly, with a tiny amount, to 0.992 for $E_{\rm I}^{\ \perp} = 100$ kJ/mol.

The low energy threshold to the reactivity is not unexpected as the corresponding normal incidence energy of 2 kJ/mol is similar to the smallest barrier height found in Table 3 (see the singly underlined minimum barrier). As discussed earlier, ⁴³ the shape of the PES and the lack of accessible rovibrational energy for the DC of O_2 means that most of the dissociation will be driven by the normal incidence energy of the molecule. Furthermore, the maximum barrier height found in Table 3 is only a few kJ/mol higher than the value of E_1^{\perp} at which the computed sticking probability appears saturated. Unlike found for the dissociation of O_2 on Cu(111), ⁷⁰ the overwhelmingly greater part (by more than 1 order of magnitude) of the DC of O_2 on Al(111) occurs via a direct mechanism (Section S2 and Figure S2 of the Supporting Information I). The minor drop in reactivity for very high E_1^{\perp} is most likely caused by an effect

similar to the bobsled effect $^{99-101}$ where the fast O_2 molecules barrel beyond the early barrier to hit a potential wall behind it and are forced to scatter back before the O_2 bond length becomes large enough for dissociation. However, it is clear that this effect is very small, and therefore not worthy of much discussion.

The QCT results based on the HSE06-1/2x-VdWDF2 DF are close to the HSE03-1/3x results of Gerrits et al. ¹⁰ The onset of sticking obtained with the HSE06-1/2x-VdWDF2 DF occurs at somewhat lower E_1^{\perp} and the saturation of the sticking occurs at a somewhat higher energy. That is, the sticking curve undergoes a slight broadening, which is expected when looking at the increased energetic corrugation of the barriers seen in Table 3 and Figure S1. Like the previous HSE03-1/3x result, the HSE06-1/2x-VdWDF2 curve represents a substantial improvement over previous GGA or mGGA-based results. The newly computed curve captures the onset of the experimentally determined S_0 very well, although it is still not able to describe the S_0 accurately for larger E_1^{\perp} .

3.3. Discussion and Future Prospects. The comparison of the quality of the different DFs is further aided by Figure 4. In

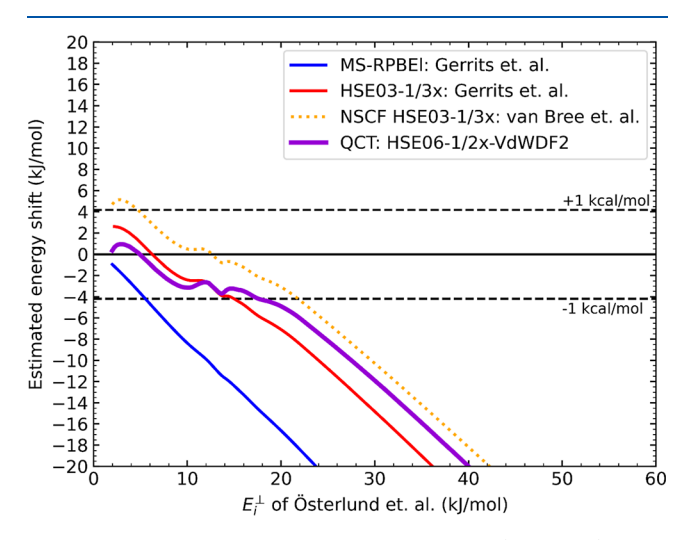


Figure 4. Estimated normal incidence energy shift (in kJ/mol) of the computed sticking probabilities relative to the experimental results of Österlund et al. ¹⁷ as a function of the normal incidence energy of the same experimental reference. The 1 kcal/mol boundary is indicated by dashed lines. Shown are results based on the MS-RPBEI DF (blue) of Gerrits et al., ¹⁰ HSE03-1/3x DF (red) of Gerrits et al., ¹⁰ the NSCF HSE03-1/3x@RPBE DF (orange dotted) of van Bree et al., ⁴³ and the HSE06-1/2x-VdWDF2 used here (purple). The *x*-axis is cut off at 60 kJ/mol and energy shifts smaller than −20 kJ/mol are not plotted for clarity of the plot.

this figure, the estimated energy shift of the S_0 curve obtained for a specific DF from the experimental curve is plotted as a function of the E_1^{\perp} of the experimental reference. This means that for any E_1^{\perp} shown on the x-axis in Figure 4, the energy shift shown on the y-axis needs to be applied to the experimental result for that E_1^{\perp} to match the S_0 values computed with the specific DF.

Figure 4 shows very clearly that the onset of the S_0 curve is described very accurately by the HSE06-1/2x-VdWDF2 DF. Even though the description of the HSE03-1/3x DF was already within chemical accuracy for the onset, the HSE06-1/2x-VdWDF2 is a better match to the experimental onset, as can also be seen in Figure 3. However, the results depicted in Figure 4 are very sobering for the impact of the combined effect of using

VdW correlation and increasing the fraction of exact exchange on the 6D dynamics. The overall improvement over the HSE03-1/3x DF is limited as both DFs quickly deviate from the experimental S_0 once the incidence energy in the experiments exceeds 22 kJ/mol. It is clear that the minor broadening of the sticking curve that resulted from the implementation of the VdW correlation, although present, is not enough to lead to agreement with experiments within chemical accuracy over the entire energy range shown.

In the end, these results raise a major question for the O2 + Al(111) system: what does this mean for the ability of DFT combined with the BOSS model to accurately describe O2 + Al(111)? For this paper, we have employed one of the least reactive forms of a screened hybrid VdW DF that can be constructed based on the generic HSE06 expression. Any reduction of the fraction of exact exchange will result in more GGA-like results, thus increasing the reactivity. Using even higher mixing ratios seems doubtful as there are formal reasons for limiting the fraction of exact exchange to values equal to 1/nwith n a whole number, n and the use of n = 1 would be completely replacing the semilocal exchange with exact exchange. Furthermore, the VdW-DF2 description of electron correlation remains one of the better methods to describe longrange molecule-metal interactions. ^{34,63} Yet, the composite DF tested here with $\alpha = 1/2$ yields only marginal improvements over the previously used screened hybrid DF with $\alpha = 1/3$. Lastly, the NSCF HSE03-1/3x@RPBE approach⁴³ yielded a larger energetic corrugation of the barrier than either SCF approach, yet still resulted in only small changes in the computed S_0 curve relative to the SCF curve. Thus, an improvement of the computed S_0 for O_2 on Al(111), by any new DF, would need to come from a larger increase of the energetic corrugation of the barrier, or another large change of an aspect of the PES of which the importance is not foreseen at present. However, the similarities between the HSE06-1/2x-VdWDF2 and HSE03-1/3x barriers cast doubt on the possibility of any other screened hybrid-based DF to achieve such radical changes. Therefore, we argue that it is unlikely that the combination of screened HF exchange with VdW correlation DFs shall result in an accurate description of the O_2 + Al(111) system if one also sticks to the use of the BOSS model for the dynamics.

To improve the accuracy of the theoretical description we could try to go beyond the hybrid level of DFT. However, we emphasize the already high computational demands of planewave screened hybrid DFT for this system and for O2 + Cu(111).⁷⁰ These high costs make the brute-force use of any higher level of theory impractical at this time. This means that DFT methods like the random phase approximation (RPA) or other types of theory like Quantum Monte Carlo remain unfeasible to be used for more than the calculation of a few barrier heights. Although these types of calculations can be insightful to benchmark a select few barrier heights, 91,103-105 such calculations will not allow for QCT dynamics to compute sticking curves. Another option to possibly improve the quality of the screened hybrid DF is to mix mGGA exchange instead of GGA exchange with exact exchange. 106,107 This type of mGGAhybrid DF is still untested for molecule-metal systems. One could also try the recent DFs in which screened exchange DFs that are tailored to and are consistent with VdW-DFs combined with them. 71,72 However, before mapping out a completely new PES with a new DF and then testing it with dynamics calculations one might also attempt the QMC-DF approach, in which one would try to reproduce the barrier height

computed with diffusion Monte Carlo by fitting a parameter in the generic, well-chosen, combination of a screened hybrid DF with a VdW correlation DF. For a proper description of the energetic barrier corrugation one might need to verify beforehand whether the energetic corrugation is well described with this approach of at least a few different barrier geometries.

If the construction of a PES at the screened hybrid or higher level of theory will remain as computationally expensive as in this work, then choosing a more advanced electronic structure method cannot be done lightly, as already explained. Thus, before trying yet another new DF or electronic structure approach to improve the description of DC of $O_2 + Al(111)$ it may be more fruitful to briefly explore the effects and limitations of the approximations made in the BOSS model. Eliminating unfounded approximation in the BOSS model may, at this point, prove computationally less demanding than any further advancements in electronic structure calculations.

Surface temperature (T_S) effects, whether associated with surface phonons or electronic excitations in the metal, remain an unlikely cause for the disagreement with experiment, as the experiments of Österlund et al.¹⁷ have shown no discernible influence of T_s on the reactivity over a T_s range of 90–650 K¹⁷. Thus, only a minor effect of surface atom displacements arising from the nonzero surface temperature in the experiments would be expected on S_0 . Furthermore, the barriers to DC are generally located early in the entrance channel, i.e., at molecule-metal distances commonly larger than 2.5 Å, which also means that the perturbation of surface atom motion due to the incoming molecule may be limited. 45,46 This suggests a limited effect of any energy loss of the impinging molecule to surface atom motion that might occur before overcoming the barrier. As an additional test, the expected upper bound of the effect surface atom motion can be calculated using the simple, Baule model¹⁰⁸ and we show the effect in Figure S3 of the Supporting Information. The Baule method treats the molecule and the surface atoms as hard spheres, and will likely result in an overestimated effect of surface atom motion. Nevertheless, Figure S3 does indicate that including surface atom motion may result in better agreement of the computed S_0 with experiments for low incidence energies, i.e., $E_{\rm I}^{\perp}$ < 26 kJ/mol. For larger $E_{\rm I}^{\perp}$ the influence of surface atom motion will likely remain too small to result in an improved agreement with experiments. Therefore, the effect of the static surface approximation, i.e., of using an ideal and static surface in the dynamical model, may be relatively

If using the static surface approximation would not have a large impact, could making the Born-Oppenheimer approximation still be a cause of concern? systems with low charge transfer energies may be more susceptible to, e.g., ehp excitation. 47,48,109 Ehp excitation is commonly modeled by the use of electronic friction techniques, 110 but the effect of electronic friction has not yet been modeled for the O2 + Al(111) system in conjunction with a PES obtained using a DF featuring screened exact exchange. One reason for this may be that there are two strong arguments against electronic friction having a substantial effect. First, the barrier is early, so the O₂ will likely not sample higher electronic densities of the metal, thus limiting the effectiveness of electronic friction. Second, electronically adiabatic calculations on DC of O2 on Ag(111),⁴⁹ in which reaction occurs at much higher energies than on Al(111), 17,49 and calculations employing the local density friction approximation (LDFA) on DC of N₂ on a metal surface 111,112 suggest that the DC of these "heavier molecule",

i.e. heavier than H₂, is not much affected by ehp excitation, likely due to the lower velocities exhibited by molecules heavier than H_2^{112} . This might seem to suggest that ehp-excitation may also have only a small influence on reducing reactivity. There are two reasons why this preliminary conclusion might not hold. First, calculations using a different electron friction model, e.g., orbital dependent friction (ODF), suggest a much larger influence of ehp excitation on DC of N_2 + Ru(0001) than calculations using the LDFA model. 112 Currently, it is not yet known which of the two electronic friction methods is best, or whether either of the two methods is accurate for modeling the effect of ehp excitation on DC on metals.³⁵ Second, for low E_{CT} systems, a strong electronically nonadiabatic effect can also occur through jumps of electrons between electronic states in which either the neutral molecule or the molecular anion interacts with the surface. 113 The nonadiabatic couplings between such states are quite strong, and modeling of the associated nonadiabaticity requires a method that is suited to deal with the associated "strongcoupling case", like the independent electron-surface hopping (IESH) method of Tully and co-workers. 114,115

An argument in favor of the BOSS model is the semi-quantitative agreement achieved with experiment of sticking probabilities computed with the BOSS model using a PES calculated with the embedded correlated wave function (ECW) approach by Yin et al., who used CASPT2 for the embedded cluster²⁴ (see also Figure 3). This would seem to suggest that an accurate sticking probability curve can be computed within the BOSS dynamical model, but leaves open the questions of whether this can be done with DFT, and how accurate the ECW method employing CASPT2 for the active site actually is.

In summary, the low $E_{\rm CT}$ of ${\rm O_2}$ + Al(111) may still imply the presence of nonadiabatic effects in the DC of ${\rm O_2}$ on Al(111) that can, per definition, not be captured by the currently employed BOSS model. Moreover, ${\rm O_2}$ incidence energy loss, whether through ehp excitation or dissipation to surface atom motion, would be expected to have its largest effect on the reactivity in the higher incidence energy range, i.e., the energy range currently most poorly described by our current BOSS-DFT approach. For future work, it should therefore be insightful to test the effect of allowing surface-atom motion, and of ehp excitation, if only for the purpose of elimination, before looking into further alterations of the DF used.

A computationally cheap method to model the effects of surface atom motion may be the dynamic corrugation method, previously successfully implemented for $H_2 + Cu(111)$. For this method, we would only need a few hundred additional DFT single-point calculations to construct the coupling potential. 116 Alternatively one could use a high-dimensional neural network (HDNN) approach to fit the PES. 117,118 The cheapest method to treat electronically nonadiabatic effects is the LDFA method, 47 but one should also test the ODF approach, 112 and possibly a recently suggested electronic friction approach called scattering potential friction.³⁵ Lastly, any future work with screened hybrid DFs will have to deal with the high computational demands. Future work could try to further reduce the amount of DFT data needed for the CRP method when building the PES, as the direct product and rigid grid now used require multiple geometries that are of limited use for fitting the dynamically relevant parts of the PES. The possibilities of a Δ -machine learning neural network approach, for example, as previously implemented for liquid water,¹ come to mind to further decrease the amount of computationally demanding calculations using a screened hybrid DF. In such

an approach one might first fit a GGA-VdW potential energy surface to a large amount of points and then upgrade to a screened hybrid-VdW quality PES by fitting and using the difference of energies computed for far lesser points. To our knowledge, such an approach has not yet been tested on the DC of molecules on metal surfaces.

Finally, one may look for errors in the procedure used by the experimentalists to estimate the sticking probabilities for O_2 at fixed energies. The experimentalists calculated what they called the "beam energy" from the known heat capacities of He, O_2 , and Xe, which is an approximate procedure. According to the experimentalists the spread in the incidence energy of the beams employed, and the rotational temperature used in an experiment were estimated from earlier work. These approximate procedures to which we compare here may all have led to errors. Given the important role of $O_2 + Al(111)$ as a benchmark system it might be useful if the experiments were repeated, with time-of-flight measurements to more accurately determine the energy distributions of He-seeded or Xe antiseeded beams and more accurate determination of their rotational and vibrational temperature than was possible before.

4. CONCLUSIONS

The combination of a DFT approach for the electronic structure of the PES and the use of the BOSS dynamical model has thus far not been able to accurately describe the DC of O_2 on Al(111). Past work has strongly suggested that this is due to the inability of the workhorse electronic structure approach in surface science, i.e., GGA-DFT, to accurately describe systems for which the charge transfer energy is below 7 eV. Although the cause of the failure of GGA-DFT is still debated, several prior works suggest that the use of hybrid DFT leads to substantial improvement in the description of systems characterized by a low charge transfer energy. Previous work on O_2 + Al(111) additionally suggested that the description of this system could be improved further by increasing the energetic corrugation of the barrier. It was believed that this could be achieved by including improved long-range, VdW-, electronic correlation while simultaneously increasing the fraction of exact exchange in the exchange-correlation DF.

To test this assumption, this paper used the HSE06-1/2x-VdWDF2 DF. This DF is a screened hybrid DF that includes a maximum admixing of $\alpha = 1/2$ of exact exchange and relies on the VdWDF2 electronic correlation description. To test this DF a 6D static surface PES was fitted to DFT energies for over five thousand different O₂ + Al(111) configurations, using the CRP. This PES was used to perform QCT dynamics calculations for different initial O₂ conditions to simulate the S₀ of O₂ on Al(111) as a function of $E_i \perp$, using the BOSS dynamical model.

The use of VdWDF2 correlation and the increase of the fraction of exact exchange results in two changes in the PES respective to the previous HSE03-1/3x screened hybrid PES. First, a VdW well now appears in the entrance channel of the PES. This well is generally only dependent on the angle of the $\rm O_2$ molecule with the surface normal. Second, the reaction barriers also change. The barriers of HSE06-1/2x-VdWDF2 in some cases shift to lower but in most cases to higher energies. This results in a slight increase of the energetic corrugation of the barrier, although the changes remain small and are smaller than the changes seen in the barriers when applying the HSE03-1/3x DF in the NSCF approach to an RPBE density, as has been done previously.

The small changes in the PES from the use of the HSE06-1/2x-VdWDF2 DF do result in some changes in the S_0 . The onset of the sticking curve moves to a somewhat lower energy and the sticking curve has undergone a slight broadening, due to the increase in the energetic corrugation of the barrier. However, the changes are not very large, and the distinction between the SCF and NSCF application of a hybrid DF is more substantial. As such, even though the changes in the PES and S_0 are as expected, the small magnitude of these changes means that the use of the HSE06-1/2x-VdWDF2 DF has not yet resulted in the desired degree of improvement of the description of sticking of O_2 on Al(111).

Furthermore, based on the comparison of the three different DF-approaches, i.e., SCF HSE03-1/3x, NSCF HSE03-1/3x@ RPBE, and HSE06-1/2x-VdWDF2, we argue that much larger changes in the PES will be required to more closely reproduce the experimental S_0 with the use of the BOSS-model. The results obtained here at high computational cost signal that it is unlikely that the combined BOSS and DFT approach, as currently implemented, can be made accurate enough for the DC of O_2 + Al(111).

Given the above, we suggest that future work on O_2 + Al(111) would first aim at eliminating the possible influences and errors associated with the dynamical approximations inherent in the BOSS model. Addressing the effects of surface atom motion can be cost-effectively done by applying the dynamical corrugation method, while one might also use the HDNN method to obtain a PES incorporating the effect of surface atom motion. The influence of electronically nonadiabatic effects like ehp excitation can be modeled with different electron friction approaches or with a method more appropriate for strong nonadiabatic electron coupling, like the IESH method, in combination with the QCT method. Future work would also do best to try and address the mounting computational costs associated with screened hybrid DFT or other higher-level electronic structure approaches. Finally, given the important role of the O_2 + Al(111) as a benchmark system, it would be good if the experiments were to be repeated to investigate the quality of the approximate procedure used by the experimentalist to arrive at initial-rovibrational-state-selective sticking probabilities for specific single incidence energies.

ASSOCIATED CONTENT

Supporting Information

The Supporting Information is available free of charge at https://pubs.acs.org/doi/10.1021/acs.jpcc.5c00327.

The first section presents a visual aid for Table 3, by plotting the barrier heights dsplayed in the table as a bar plot. The second section is a brief overview of the deconvolution of the indirect and direct reaction mechanism as simulated in the QCT calculations and shows that an indirect mechanism has a minor and negligible contribution to the total sticking probability. The third section briefly discusses the Baule model to molecule-metal surface energy transfer and presents a figure showing an expected lower bound for the reactivity of the $\rm O_2 + Al(111)$ system if energy transfer to the Al surface phonons were to be included (PDF)

AUTHOR INFORMATION

Corresponding Authors

- R. A. B. van Bree Leiden Institute of Chemisty, Leiden University, Leiden 2300 RA, The Netherlands; orcid.org/0000-0003-1393-9650; Email: r.a.b.van.bree@lic.leidenuniv.nl
- G. J. Kroes Leiden Institute of Chemisty, Leiden University, Leiden 2300 RA, The Netherlands; oorcid.org/0000-0002-4913-4689; Email: g.j.kroes@chem.leidenuniv.nl

Complete contact information is available at: https://pubs.acs.org/10.1021/acs.jpcc.5c00327

Author Contributions

Conceptualization: R.A.B. van Bree, G.J. Kroes; Data curation: R.A.B. van Bree; Formal Analysis: R.A.B. van Bree; Funding acquisition: G.J. Kroes; Investigation: R.A.B. van Bree; Methodology: R.A.B. van Bree; Project administration: G.J. Kroes; Resources: G.J. Kroes; Software: R.A.B. van Bree; Supervision: G.J. Kroes; Validation: R.A.B. van Bree, G.J. Kroes; Visualization: R.A.B. van Bree; Writing—original draft: R.A.B. van Bree; Writing—review and editing: R.A.B. van Bree, G.J. Kroes.

Notes

The authors declare no competing financial interest.

ACKNOWLEDGMENTS

We acknowledge the Leiden Institute of Chemistry for the project funding and acknowledge the NWO-EW 2021.12 supercomputer grant for the supercomputer time. We thank Nick Gerrits for the discussions on DF choice and $O_2 + Al(111)$. We also thank Jonathon Cottom for useful discussions. We thank Floris Löffler for his exploratory investigation of the barrier heights produced by the HSE06-1/2x-VdWDF2 DF for $O_2 + Al(111)$. Lastly, we thank Mark Somers for managing the high-performance computing infrastructure of the group.

REFERENCES

- (1) Ertl, G. Elementary Steps in Heterogeneous Catalysis. Angew. Chem., Int. Ed. Engl. 1990, 29 (11), 1219–1227.
- (2) Sabbe, M. K.; Reyniers, M.-F.; Reuter, K. First-Principles Kinetic Modeling in Heterogeneous Catalysis: An Industrial Perspective on Best-Practice, Gaps and Needs. *Catal. Sci. Technol.* **2012**, *2* (10), 2010–2024
- (3) Wolcott, C. A.; Medford, A. J.; Studt, F.; Campbell, C. T. Degree of Rate Control Approach to Computational Catalyst Screening. *J. Catal.* **2015**, *330*, 197–207.
- (4) Gartland, P. O. Adsorption of Oxygen on Clean Single Crystal Faces of Aluminium. Surf. Sci. 1977, 62 (1), 183–196.
- (5) Roberts, M. W. Chemisorption and Reaction Pathways at Metal Surfaces: The Role of Surface Oxygen. *Chem. Soc. Rev.* **1989**, *18*, 451–475.
- (6) Lundgren, E.; Mikkelsen, A.; Andersen, J. N.; Kresse, G.; Schmid, M.; Varga, P. Surface Oxides on Close-Packed Surfaces of Late Transition Metals. *J. Phys.: Condens. Matter* **2006**, *18* (30), R481–R499.
- (7) Montemore, M. M.; van Spronsen, M. A.; Madix, R. J.; Friend, C. M. O 2 Activation by Metal Surfaces: Implications for Bonding and Reactivity on Heterogeneous Catalysts. *Chem. Rev.* **2018**, *118* (5), 2816–2862.
- (8) Behler, J.; Delley, B.; Lorenz, S.; Reuter, K.; Scheffler, M. Dissociation of O2 at Al(111): The Role of Spin Selection Rules. *Phys. Rev. Lett.* **2005**, 94 (3), 036104.
- (9) Cheng, J.; Libisch, F.; Carter, E. A. Dissociative Adsorption of O 2 on Al(111): The Role of Orientational Degrees of Freedom. *J. Phys. Chem. Lett.* **2015**, *6* (9), 1661–1665.

- (10) Gerrits, N.; Smeets, E. W. F.; Vuckovic, S.; Powell, A. D.; Doblhoff-Dier, K.; Kroes, G.-J. Density Functional Theory for Molecule—Metal Surface Reactions: When Does the Generalized Gradient Approximation Get It Right, and What to Do If It Does Not. *J. Phys. Chem. Lett.* **2020**, *11* (24), 10552–10560.
- (11) Ertl, G. Reactions at Surfaces: From Atoms to Complexity (Nobel Lecture). *Angew. Chemie Int. Ed.* **2008**, 47 (19), 3524–3535.
- (12) Jacobsen, J.; Hammer, B.; Jacobsen, K. W.; No/rskov, J. K. Electronic Structure, Total Energies, and STM Images of Clean and Oxygen-Covered Al(111). *Phys. Rev. B* **1995**, 52 (20), 14954–14962.
- (13) Kroes, G.-J.; Díaz, C. Quantum and Classical Dynamics of Reactive Scattering of H₂ from Metal Surfaces. *Chem. Soc. Rev.* **2016**, 45 (13), 3658–3700.
- (14) Kroes, G.-J. Computational Approaches to Dissociative Chemisorption on Metals: Towards Chemical Accuracy. *Phys. Chem. Chem. Phys.* **2021**, 23 (15), 8962–9048.
- (15) Batra, I. P.; Kleinman, L. Chemisorption of Oxygen on Aluminum Surfaces. *J. Electron Spectrosc. Relat. Phenom.* **1984**, 33 (3), 175–241.
- (16) Kerkar, M.; Fisher, D.; Woodruff, D. P.; Cowie, B. Adsorption Site Determination for Oxygen on Al(111) Using Normal Incidence Standing X-Ray Wavefield Absorption. *Surf. Sci.* **1992**, 271 (1–2), 45–56.
- (17) Österlund, L.; Zoric-acute, I.; Kasemo, B. Dissociative Sticking of O2 on Al(111). *Phys. Rev. B* **1997**, *55* (23), 15452–15455.
- (18) Zhukov, V.; Popova, I.; Yates, J. T. Initial Stages of Al(111) Oxidation with Oxygen-Temperature Dependence of the Integral Reactive Sticking Coefficient. *Surf. Sci.* 1999, 441 (2–3), 251–264.
- (19) Liu, H.-R.; Xiang, H.; Gong, X. G. First Principles Study of Adsorption of O 2 on Al Surface with Hybrid Functionals. *J. Chem. Phys.* **2011**, *135* (21), 214702.
- (20) Kurahashi, M.; Yamauchi, Y. Steric Effect in O2 Sticking on Al(111): Preference for Parallel Geometry. *Phys. Rev. Lett.* **2013**, *110* (24), 246102.
- (21) Smits, B.; Somers, M. F. The Quantum Dynamics of H2 on Cu(111) at a Surface Temperature of 925 K: Comparing State-of-the-Art Theory to State-of-the-Art Experiments. *J. Chem. Phys.* **2022**, *157* (13), 134704.
- (22) Díaz, C.; Pijper, E.; Olsen, R. A.; Busnengo, H. F.; Auerbach, D. J.; Kroes, G. J. Chemically Accurate Simulation of a Prototypical Surface Reaction: H2 Dissociation on Cu(111). *Science* **2009**, *326* (5954), 832–834.
- (23) Libisch, F.; Huang, C.; Liao, P.; Pavone, M.; Carter, E. A. Origin of the Energy Barrier to Chemical Reactions of O2 on Al(111): Evidence for Charge Transfer, Not Spin Selection. *Phys. Rev. Lett.* **2012**, *109* (19), 198303.
- (24) Yin, R.; Zhang, Y.; Libisch, F.; Carter, E. A.; Guo, H.; Jiang, B. Dissociative Chemisorption of O 2 on Al(111): Dynamics on a Correlated Wave-Function-Based Potential Energy Surface. *J. Phys. Chem. Lett.* **2018**, *9* (12), 3271–3277.
- (25) Fan, X. L.; Lau, W. M.; Liu, Z. F. Comment on "Dissociation of O2 at Al(111): The Role of Spin Selection Rules. *Phys. Rev. Lett.* **2006**, 96 (7), 079801.
- (26) Behler, J.; Reuter, K.; Scheffler, M. Behler, Reuter, and Scheffler Reply. *Phys. Rev. Lett.* **2006**, *96* (7), 79802.
- (27) Carbogno, C.; Behler, J.; Groß, A.; Reuter, K. Fingerprints for Spin-Selection Rules in the Interaction Dynamics of O2 at Al(111). *Phys. Rev. Lett.* **2008**, *101* (9), 096104.
- (28) Carbogno, C.; Behler, J.; Reuter, K.; Groß, A. Signatures of Nonadiabatic O2- Dissociation at Al(111): First-Principles Fewest-Switches Study. *Phys. Rev. B* **2010**, *81* (3), 035410.
- (29) Behler, J.; Reuter, K.; Scheffler, M. Nonadiabatic Effects in the Dissociation of Oxygen Molecules at the Al(111) Surface. *Phys. Rev. B* **2008**, 77 (11), 115421.
- (30) Sasaki, T.; Ohno, T. Calculations of the Potential-Energy Surface for Dissociation Process of O2 on the Al(111) Surface. *Phys. Rev. B* **1999**, *60* (11), 7824–7827.
- (31) Honkala, K.; Laasonen, K. Oxygen Molecule Dissociation on the Al(111) Surface. *Phys. Rev. Lett.* **2000**, *84* (4), 705–708.

- (32) Yourdshahyan, Y.; Razaznejad, B.; Lundqvist, B. I. Adiabatic Potential-Energy Surfaces for Oxygen on Al(111). *Phys. Rev. B* **2002**, *65* (7), 075416.
- (33) Hammer, B.; Hansen, L. B.; Nørskov, J. K. Improved Adsorption Energetics within Density-Functional Theory Using Revised Perdew-Burke-Ernzerhof Functionals. *Phys. Rev. B* **1999**, *59* (11), 7413–7421.
- (34) Tchakoua, T.; Gerrits, N.; Smeets, E. W. F.; Kroes, G.-J. SBH17: Benchmark Database of Barrier Heights for Dissociative Chemisorption on Transition Metal Surfaces. *J. Chem. Theory Comput.* **2023**, 19 (1), 245–270.
- (35) Kroes, G.; Meyer, J. Best-of-Both-Worlds Computational Approaches to Difficult-to-Model Dissociation Reactions on Metal Surfaces. *Chem. Sci.* **2025**, *16* (2), 480–506.
- (36) Perdew, J. P. Climbing the Ladder of Density Functional Approximations. MRS Bull. 2013, 38 (9), 743–750.
- (37) Kim, M.-C.; Sim, E.; Burke, K. Understanding and Reducing Errors in Density Functional Calculations. *Phys. Rev. Lett.* **2013**, *111* (7), 073003.
- (38) Sim, E.; Song, S.; Burke, K. Quantifying Density Errors in DFT. *J. Phys. Chem. Lett.* **2018**, 9 (22), 6385–6392.
- (39) Vuckovic, S.; Song, S.; Kozlowski, J.; Sim, E.; Burke, K. Density Functional Analysis: The Theory of Density-Corrected DFT. *J. Chem. Theory Comput.* **2019**, *15* (12), *6636–6646*.
- (40) Song, S.; Vuckovic, S.; Sim, E.; Burke, K. Density Sensitivity of Empirical Functionals. *J. Phys. Chem. Lett.* **2021**, 12 (2), 800–807.
- (41) Kaplan, A. D.; Shahi, C.; Bhetwal, P.; Sah, R. K.; Perdew, J. P. Understanding Density-Driven Errors for Reaction Barrier Heights. *J. Chem. Theory Comput.* **2023**, *19* (2), 532–543.
- (42) Kanungo, B.; Kaplan, A. D.; Shahi, C.; Gavini, V.; Perdew, J. P. Unconventional Error Cancellation Explains the Success of Hartree–Fock Density Functional Theory for Barrier Heights. *J. Phys. Chem. Lett.* **2024**, *15* (1), 323–328.
- (43) van Bree, R. A. B.; Gerrits, N.; Kroes, G.-J. Dissociative Chemisorption of O 2 on Al(111): Dynamics on a Potential Energy Surface Computed with a Non-Self-Consistent Screened Hybrid Density Functional Approach. *Faraday Discuss.* **2024**, *251*, 361–381.
- (44) Gerrits, N.; Smeets, E. W. F.; Vuckovic, S.; Powell, A. D.; Doblhoff-Dier, K.; Kroes, G.-J. Correction to "Density Functional Theory for Molecule—Metal Surface Reactions: When Does the Generalized Gradient Approximation Get It Right, and What to Do If It Does Not. J. Phys. Chem. Lett. 2022, 13 (45), 10575–10576.
- (45) Tiwari, A. K.; Nave, S.; Jackson, B. Methane Dissociation on Ni(111): A New Understanding of the Lattice Effect. *Phys. Rev. Lett.* **2009**, *103* (25), 253201.
- (46) Tiwari, A. K.; Nave, S.; Jackson, B. The Temperature Dependence of Methane Dissociation on Ni(111) and Pt(111): Mixed Quantum-Classical Studies of the Lattice Response. *J. Chem. Phys.* **2010**, *132* (13), 134702.
- (47) Juaristi, J. I.; Alducin, M.; Muiño, R. D.; Busnengo, H. F.; Salin, A. Role of Electron-Hole Pair Excitations in the Dissociative Adsorption of Diatomic Molecules on Metal Surfaces. *Phys. Rev. Lett.* **2008**, *100* (11), 116102.
- (48) Spiering, P.; Meyer, J. Testing Electronic Friction Models: Vibrational De-Excitation in Scattering of H2 and D2 from Cu(111). *J. Phys. Chem. Lett.* **2018**, 9 (7), 1803–1808.
- (49) Goikoetxea, I.; Beltrán, J.; Meyer, J.; Iñaki Juaristi, J.; Alducin, M.; Reuter, K. Non-Adiabatic Effects during the Dissociative Adsorption of O 2 at Ag(111)? A First-Principles Divide and Conquer Study. *New J. Phys.* **2012**, *14* (1), 013050.
- (50) Wijzenbroek, M.; Kroes, G. J. The Effect of the Exchange-Correlation Functional on H2 Dissociation on Ru(0001). *J. Chem. Phys.* **2014**, *140* (8), 084702.
- (51) Karikorpi, M.; Holloway, S.; Henriksen, N.; Nørskov, J. K. Dynamics of Molecule-Surface Interactions. *Surf. Sci. Lett.* **1987**, *179* (1), L41–L48.
- (52) Migliorini, D.; Nattino, F.; Kroes, G.-J. Application of van Der Waals Functionals to the Calculation of Dissociative Adsorption of N2 on W(110) for Static and Dynamic Systems. *J. Chem. Phys.* **2016**, 144 (8), 084702.

- (53) Dion, M.; Rydberg, H.; Schröder, E.; Langreth, D. C.; Lundqvist, B. I. Van Der Waals Density Functional for General Geometries. *Phys. Rev. Lett.* **2004**, 92 (24), 246401.
- (54) Lee, K.; Murray, E. D.; Kong, L.; Lundqvist, B. I.; Langreth, D. C. Higher-Accuracy van Der Waals Density Functional. *Phys. Rev. B Condens. Matter Mater. Phys.* **2010**, 82 (8), 3–6.
- (55) Heyd, J.; Scuseria, G. E.; Ernzerhof, M. Hybrid Functionals Based on a Screened Coulomb Potential. *J. Chem. Phys.* **2003**, *118* (18), 8207–8215.
- (56) Heyd, J.; Scuseria, G. E.; Ernzerhof, M. E. Erratum: "Hybrid functionals based on a screened Coulomb potential" [J. Chem. Phys. 118, 8207 (2003)]. *J. Chem. Phys.* 2006, 124 (21), 219906.
- (57) Grimme, S. Semiempirical GGA-type Density Functional Constructed with a Long-range Dispersion Correction. *J. Comput. Chem.* **2006**, 27 (15), 1787–1799.
- (58) Grimme, S.; Antony, J.; Ehrlich, S.; Krieg, H. A Consistent and Accurate Ab Initio Parametrization of Density Functional Dispersion Correction (DFT-D) for the 94 Elements H-Pu. *J. Chem. Phys.* **2010**, 132 (15), 154104.
- (59) Lundqvist, B. I.; Andersson, Y.; Shao, H.; Chan, S.; Langreth, D. C. Density Functional Theory Including Van Der Waals Forces. *Int. J. Quantum Chem.* **1995**, *56* (4), 247–255.
- (60) Vydrov, O. A.; Van Voorhis, T. Nonlocal van Der Waals Density Functional: The Simpler the Better. *J. Chem. Phys.* **2010**, *133* (24), 244103
- (61) Sabatini, R.; Gorni, T.; de Gironcoli, S. Nonlocal van Der Waals Density Functional Made Simple and Efficient. *Phys. Rev. B* **2013**, 87 (4), 041108.
- (62) Berland, K.; Cooper, V. R.; Lee, K.; Schröder, E.; Thonhauser, T.; Hyldgaard, P.; Lundqvist, B. I. Van Der Waals Forces in Density Functional Theory: A Review of the VdW-DF Method. *Rep. Prog. Phys.* **2015**, 78 (6), 066501.
- (63) Smeets, E. W. F.; Kroes, G.-J. Designing New SRP Density Functionals Including Non-Local VdW-DF2 Correlation for H 2 + Cu(111) and Their Transferability to H 2 + Ag(111), Au(111) and Pt(111). *Phys. Chem. Chem. Phys.* **2021**, 23 (13), 7875–7901.
- (64) Perdew, J. P.; Burke, K.; Ernzerhof, M. Generalized Gradient Approximation Made Simple. *Phys. Rev. Lett.* **1996**, 77 (18), 3865–3868.
- (65) Adamo, C.; Barone, V. Toward Reliable Density Functional Methods without Adjustable Parameters: The PBE0Model. *J. Chem. Phys.* **1999**, *110* (13), 6158–6170.
- (66) Gao, W.; Abtew, T. A.; Cai, T.; Sun, Y. Y.; Zhang, S.; Zhang, P. On the Applicability of Hybrid Functionals for Predicting Fundamental Properties of Metals. *Solid State Commun.* **2016**, 234–235, 10–13.
- (67) Cohen, A. J.; Mori-Sánchez, P.; Yang, W. Challenges for Density Functional Theory. *Chem. Rev.* **2012**, *112* (1), 289–320.
- (68) Mardirossian, N.; Head-Gordon, M. Thirty Years of Density Functional Theory in Computational Chemistry: An Overview and Extensive Assessment of 200 Density Functionals. *Mol. Phys.* **2017**, *115* (19), 2315–2372.
- (69) Moldabekov, Z. A.; Lokamani, M.; Vorberger, J.; Cangi, A.; Dornheim, T. Non-Empirical Mixing Coefficient for Hybrid XC Functionals from Analysis of the XC Kernel. *J. Phys. Chem. Lett.* **2023**, 14 (5), 1326–1333.
- (70) van Bree, R. A. B.; Kroes, G. J. O 2 Dissociation on Cu(111) Dynamics on a Novel Screened Hybrid van Der Waals DFT Potential Energy Surface. *J. Phys. Chem. C* **2024**, *128* (45), 19182–19196.
- (71) Shukla, V.; Jiao, Y.; Lee, J.; Schröder, E.; Neaton, J. B.; Hyldgaard, P. Accurate Nonempirical Range-Separated Hybrid van Der Waals Density Functional for Complex Molecular Problems, Solids, and Surfaces. *Phys. Rev. X* **2022**, *12* (4), 041003.
- (72) Shukla, V.; Jiao, Y.; Frostenson, C. M.; Hyldgaard, P. VdW-DF-Ahcx: A Range-Separated van Der Waals Density Functional Hybrid. *J. Phys.: Condens. Matter* **2022**, 34 (2), 025902.
- (73) Kresse, G.; Hafner, J. Ab Initio Molecular Dynamics for Liquid Metals. *Phys. Rev. B* **1993**, *47* (1), 558–561.

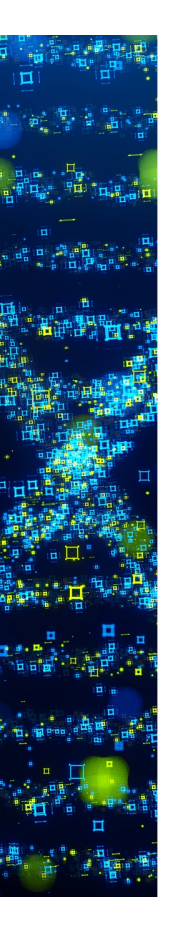
- (74) Kresse, G.; Hafner, J. Norm-Conserving and Ultrasoft Pseudopotentials for First-Row and Transition Elements. *J. Phys.: Condens. Matter* **1994**, *6* (40), 8245–8257.
- (75) Kresse, G.; Hafner, J. Ab Initio Molecular-Dynamics Simulation of the Liquid-Metal–Amorphous-Semiconductor Transition in Germanium. *Phys. Rev. B* **1994**, *49* (20), 14251–14269.
- (76) Kresse, G.; Furthmüller, J. Efficiency of Ab-Initio Total Energy Calculations for Metals and Semiconductors Using a Plane-Wave Basis Set. *Comput. Mater. Sci.* **1996**, *6* (1), 15–50.
- (77) Kresse, G.; Furthmüller, J. Efficient Iterative Schemes for Ab Initio Total-Energy Calculations Using a Plane-Wave Basis Set. *Phys. Rev. B* **1996**, 54 (16), 11169–11186.
- (78) Kresse, G.; Joubert, D. From Ultrasoft Pseudopotentials to the Projector Augmented-Wave Method. *Phys. Rev. B* **1999**, *59* (3), 1758–1775.
- (79) Klimeš, J.; Bowler, D. R.; Michaelides, A. A Critical Assessment of Theoretical Methods for Finding Reaction Pathways and Transition States of Surface Processes. *J. Phys.: Condens. Matter* **2010**, 22 (7), 074203.
- (80) Klimeš, J.; Bowler, D. R.; Michaelides, A. Van Der Waals Density Functionals Applied to Solids. *Phys. Rev. B* **2011**, 83 (19), 195131.
- (81) Blöchl, P. E. Projector Augmented-Wave Method. *Phys. Rev. B* **1994**, *S0* (24), 17953–17979.
- (82) Teter, M. P.; Payne, M. C.; Allan, D. C. Solution of Schrödinger's Equation for Large Systems. *Phys. Rev. B* **1989**, 40 (18), 12255–12263.
- (83) Bylander, D. M.; Kleinman, L.; Lee, S. Self-Consistent Calculations of the Energy Bands and Bonding Properties of B12C3. *Phys. Rev. B* **1990**, 42 (2), 1394–1403.
- (84) PRECFOCK VASP Wiki. https://www.vasp.at/wiki/index.php/PRECFOCK (accessed 13-01 2025).
- (85) Haas, P.; Tran, F.; Blaha, P. Calculation of the Lattice Constant of Solids with Semilocal Functionals. *Phys. Rev. B* **2009**, *79* (8), 085104.
- (86) Noonan, J. R.; Davis, H. L. Confirmation of an Exception to the "General Rule" of Surface Relaxations. *J. Vac. Sci. Technol. A Vacuum, Surfaces, Film.* **1990**, 8 (3), 2671–2676.
- (87) Schöchlin, J.; Bohnen, K. P.; Ho, K. M. Structure and Dynamics at the Al(111)-Surface. Surf. Sci. 1995, 324 (2–3), 113–121.
- (88) Busnengo, H. F.; Salin, A.; Dong, W. Representation of the 6D Potential Energy Surface for a Diatomic Molecule near a Solid Surface. *J. Chem. Phys.* **2000**, *112* (17), 7641–7651.
- (89) Olsen, R. A.; Busnengo, H. F.; Salin, A.; Somers, M. F.; Kroes, G. J.; Baerends, E. J. Constructing Accurate Potential Energy Surfaces for a Diatomic Molecule Interacting with a Solid Surface: H2+Pt(111) and H2+Cu(100). *J. Chem. Phys.* **2002**, *116* (9), 3841–3855.
- (90) Smeets, E. W. F.; Kroes, G. J. Performance of Made Simple Meta-GGA Functionals with RVV10 Nonlocal Correlation for H2 + Cu(111), D2 + Ag(111), H2 + Au(111), and D2 + Pt(111). *J. Phys. Chem. C* 2021, 125 (17), 8993–9010.
- (91) Powell, A. D.; Gerrits, N.; Tchakoua, T.; Somers, M. F.; Busnengo, H. F.; Meyer, J.; Kroes, G.; Doblhoff-Dier, K. Best-of-Both-Worlds Predictive Approach to Dissociative Chemisorption on Metals. *J. Phys. Chem. Lett.* **2024**, *15*, 307–315.
- (92) Wijzenbroek, M.; Klein, D. M.; Smits, B.; Somers, M. F.; Kroes, G. J. Performance of a Non-Local van Der Waals Density Functional on the Dissociation of H2 on Metal Surfaces. *J. Phys. Chem. A* **2015**, *119* (50), 12146–12158.
- (93) Karplus, M.; Porter, R. N.; Sharma, R. D. Exchange Reactions with Activation Energy. I. Simple Barrier Potential for (H, H 2). *J. Chem. Phys.* **1965**, 43 (9), 3259–3287.
- (94) Raff, L. M.; Karplus, M. Theoretical Investigations of Reactive Collisions in Molecular Beams: K+CH 3 I and Related Systems. *J. Chem. Phys.* **1966**, 44 (3), 1212–1229.
- (95) Gerrits, N.; Geweke, J.; Smeets, E. W. F.; Voss, J.; Wodtke, A. M.; Kroes, G.-J. Closing the Gap Between Experiment and Theory: Reactive Scattering of HCl from Au(111). *J. Phys. Chem. C* **2020**, *124* (29), 15944–15960.
- (96) King, D. A.; Wells, M. G. Molecular Beam Investigation of Adsorption Kinetics on Bulk Metal Targets: Nitrogen on Tungsten. *Surf. Sci.* 1972, 29 (2), 454–482.

- (97) Kuebler, N. A.; Robin, M. B.; Yang, J. J.; Gedanken, A.; Herrick, D. R. Fully Resolved Zeeman Pattern in the Stern-Gerlach Deflection Spectrum of O2 (3g-, K=1). *Phys. Rev. A* **1988**, 38 (2), 737–749.
- (98) Füchsel, G.; Del Cueto, M.; Díaz, C.; Kroes, G. J. Enigmatic HCl + Au(111) Reaction: A Puzzle for Theory and Experiment. *J. Phys. Chem. C* 2016, 120 (45), 25760–25779.
- (99) Polanyi, J. C. Some Concepts in Reaction Dynamics. *Science* **1987**, 236 (4802), 680–690.
- (100) Marcus, R. A. On the Analytical Mechanics of Chemical Reactions. Classical Mechanics of Linear Collisions. *J. Chem. Phys.* **1966**, 45 (12), 4500–4504.
- (101) McCullough, E. A.; Wyatt, R. E. Quantum Dynamics of the Collinear (H, H2) Reaction. *J. Chem. Phys.* **1969**, *S1* (3), 1253–1254. (102) Perdew, J. P.; Ernzerhof, M.; Burke, K. Rationale for Mixing
- Exact Exchange with Density Functional Approximations. *J. Chem. Phys.* **1996**, 105 (22), 9982–9985. (103) Doblhoff-Dier, K.; Meyer, J.; Hoggan, P. E.; Kroes, G.-J.
- (103) Doblhoft-Dier, K.; Meyer, J.; Hoggan, P. E.; Kroes, G.-J. Quantum Monte Carlo Calculations on a Benchmark Molecule—Metal Surface Reaction: H 2 + Cu(111). *J. Chem. Theory Comput.* **2017**, *13* (7), 3208–3219.
- (104) Oudot, B.; Doblhoff-Dier, K. Reaction Barriers at Metal Surfaces Computed Using the Random Phase Approximation: Can We Beat DFT in the Generalized Gradient Approximation? *J. Chem. Phys.* **2024**, *161* (5), 054708.
- (105) Wei, Z.; Martirez, J. M. P.; Carter, E. A. Introducing the Embedded Random Phase Approximation: H2 Dissociative Adsorption on Cu(111) as an Exemplar. *J. Chem. Phys.* **2023**, *159* (19), 194108.
- (106) Goerigk, L.; Grimme, S. Efficient and Accurate Double-Hybrid-Meta-GGA Density Functionals—Evaluation with the Extended GMTKN30 Database for General Main Group Thermochemistry, Kinetics, and Noncovalent Interactions. *J. Chem. Theory Comput.* **2011**, 7 (2), 291–309.
- (107) Brütting, M.; Bahmann, H.; Kümmel, S. Hybrid Functionals with Local Range Separation: Accurate Atomization Energies and Reaction Barrier Heights. *J. Chem. Phys.* **2022**, *156* (10), 104109.
- (108) Baule, B. Theoretische Behandlung Der Erscheinungen in Verdünnten Gasen. Ann. Phys. 1914, 349 (9), 145–176.
- (109) Golibrzuch, K.; Bartels, N.; Auerbach, D. J.; Wodtke, A. M. The Dynamics of Molecular Interactions and Chemical Reactions at Metal Surfaces: Testing the Foundations of Theory. *Annu. Rev. Phys. Chem.* **2015**, *66* (1), 399–425.
- (110) Head-Gordon, M.; Tully, J. C. Molecular Dynamics with Electronic Frictions. *J. Chem. Phys.* **1995**, *103* (23), 10137–10145.
- (111) Alducin, M.; Díez Muiño, R.; Juaristi, J. I. Non-Adiabatic Effects in Elementary Reaction Processes at Metal Surfaces. *Prog. Surf. Sci.* **2017**, 92 (4), 317–340.
- (112) Spiering, P.; Shakouri, K.; Behler, J.; Kroes, G. J.; Meyer, J. Orbital-Dependent Electronic Friction Significantly Affects the Description of Reactive Scattering of N2 from Ru(0001). *J. Phys. Chem. Lett.* **2019**, *10* (11), 2957–2962.
- (113) White, J. D.; Chen, J.; Matsiev, D.; Auerbach, D. J.; Wodtke, A. M. Conversion of Large-Amplitude Vibration to Electron Excitation at a Metal Surface. *Nature* **2005**, *4*33 (7025), 503–505.
- (114) Shenvi, N.; Roy, S.; Tully, J. C. Nonadiabatic Dynamics at Metal Surfaces: Independent-Electron Surface Hopping. *J. Chem. Phys.* **2009**, 130 (17), 174107.
- (115) Shenvi, N.; Roy, S.; Tully, J. C. Dynamical Steering and Electronic Excitation in NO Scattering from a Gold Surface. *Science* **2009**, 326 (5954), 829–832.
- (116) Smits, B.; Somers, M. F. Beyond the Static Corrugation Model: Dynamic Surfaces with the Embedded Atom Method. *J. Chem. Phys.* **2021**, *154* (7), 074710.
- (117) Shakouri, K.; Behler, J.; Meyer, J.; Kroes, G.-J. Accurate Neural Network Description of Surface Phonons in Reactive Gas—Surface Dynamics: N 2 + Ru(0001). *J. Phys. Chem. Lett.* **2017**, 8 (10), 2131—2136.
- (118) Liu, Q.; Zhou, X.; Zhou, L.; Zhang, Y.; Luo, X.; Guo, H.; Jiang, B. Constructing High-Dimensional Neural Network Potential Energy

Surfaces for Gas—Surface Scattering and Reactions. J. Phys. Chem. C 2018, 122 (3), 1761–1769.

(119) Daru, J.; Forbert, H.; Behler, J.; Marx, D. Coupled Cluster Molecular Dynamics of Condensed Phase Systems Enabled by Machine Learning Potentials: Liquid Water Benchmark. *Phys. Rev. Lett.* **2022**, 129 (22), 226001.

(120) Scoles, G. Atomic and Molecular Beam Methods; Oxford University Press, 1988; Vol. 1.



CAS BIOFINDER DISCOVERY PLATFORM™

STOP DIGGING THROUGH DATA —START MAKING DISCOVERIES

CAS BioFinder helps you find the right biological insights in seconds

Start your search

